Research in Astronomy and Astrophysics, 23:015017 (18pp), 2023 January https://doi.org/10.1088/1674-4527/aca583

The Significance of Thermally Pulsing Asymptotic Giant Branch Stars in Post-starburst Galaxies

Siqi Liu[1,2] and A-Li Luo[1,2,3]
[1] CAS Key Laboratory of Optical Astronomy, National Astronomical Observatories, Beijing 100101, China; lal@nao.cas.cn
[2] University of Chinese Academy of Sciences, Beijing 100049, China
[3] College of Computer and Information Management & Institute for Astronomical Science, Dezhou University, Dezhou 253023, China
Received 2022 September 27; revised 2022 November 20; accepted 2022 November 22; published 2023 January 11

Abstract

We measure the significance of thermally pulsing asymptotic giant branch (TP-AGB) stars via the spectral energy distributions (SEDs) of a sample of post-starburst (PSB) galaxies at $z = 0.2$–0.7. Using ground- and space-based photometry from the 3D-HST catalog, as well as associated near-infrared (NIR) Hubble Space Telescope (HST) slitless grism spectroscopy, we evaluate the importance of TP-AGB stars in the SEDs of 177 PSB galaxies by fitting simple stellar populations with different levels of TP-AGB contributions. The grism spectra, despite their low resolution of $R \sim 100$, enable the detection of molecular features specific to TP-AGB stars and thus improve constraints on their contribution. A majority (∼70%) of galaxies in the PSB sample show features indicative of TP-AGB stars, while the remainder does not and they are well fit by Bruzual & Charlot TP-AGB light models. Stacked spectra of sources classified to be the best fit by TP-AGB heavy/mild models reveal strong detections of NIR molecular features associated with TP-AGB stars. Additionally, we observe a tentative trend with redshift where more TP-AGB heavy galaxies are observed in the higher redshift PSB galaxy population. Finally, neglecting the contribution of TP-AGB stars can yield an over-prediction of stellar masses measured in the K-band ranging from 0.13–0.23 dex.

Key words: stars: AGB and post-AGB – galaxies: stellar content – galaxies: peculiar

1. Introduction

The thermally pulsing asymptotic giant branch (TP-AGB) phase is the late evolutionary stage of low- and intermediate-mass stars (0.8–8 $M_\odot$). The luminosity contribution of TP-AGB stars can be significant in the integrated stellar light of galaxies in the near-infrared (NIR) (Frogel et al. 1990; Maraston et al. 2006; Melbourne et al. 2012), due to their high intrinsic luminosity. However, because of the highly variable luminosity (due to their pulsing nature), extremely short duration of this particular pulsing phase (∼Myr), mass loss at the late stage (10^{-8}–10^{-4} $M_\odot$ yr^{-1}) (Vassiliadis & Wood 1993) and unknown levels of dust obscuration, it is challenging to theoretically model their luminosity contributions to the overall stellar light output.

The seminal work measuring the fractional luminosity of TP-AGB stars as a function of age was carried out by Frogel et al. (1990) through stellar counts of TP-AGB stars in stellar clusters within the Magellanic Clouds (MCs). When unable to resolve individual stars, as is the case of galaxies outside of our Local Group, the presence of TP-AGB stars is inferred from galaxy spectral energy distributions (SEDs). Stellar population synthesis (SPS) (Tinsley & Gunn 1976) is a commonly employed method to determine the physical properties of galaxies such as stellar age, mass, etc. Evolutionary population synthesis is a powerful technique to infer the physical properties of galaxies with the knowledge of stellar evolution from observables (spectroscopy and photometry). This requires the fitting of stellar population models with observed integrated spectra of individual galaxies. For these reasons, the observational calibration of TP-AGB stars is essential to obtain a better understanding of their contributions to galaxies. The contribution of TP-AGB stars in the emission of galaxies is based largely on the calibration carried out using the number counts of TP-AGB stars found in the MCs.

To construct stellar population models, two methods are traditionally applied to treat the late stages of stellar evolution: the isochrone synthesis technique (TP-AGB light; Bruzual & Charlot 2003) and the fuel consumption theorem (TP-AGB heavy and TP-AGB mild; Maraston 2005; Capozzi et al. 2016). The TP-AGB light model sums up the contributions to the flux of all mass bins along one isochrone by integrating the lifetime of each phase, with a specified initial mass function (IMF) and a stellar spectral library. The TP-AGB heavy model is constructed based on the principle that the mass of the fuel (mainly H/He) is converted into the total luminosity. Therefore, the TP-AGB light model essentially neglects the TP-AGB contribution because of the short duration of this stage (Bruzual & Charlot 2003). According to the prescription described in

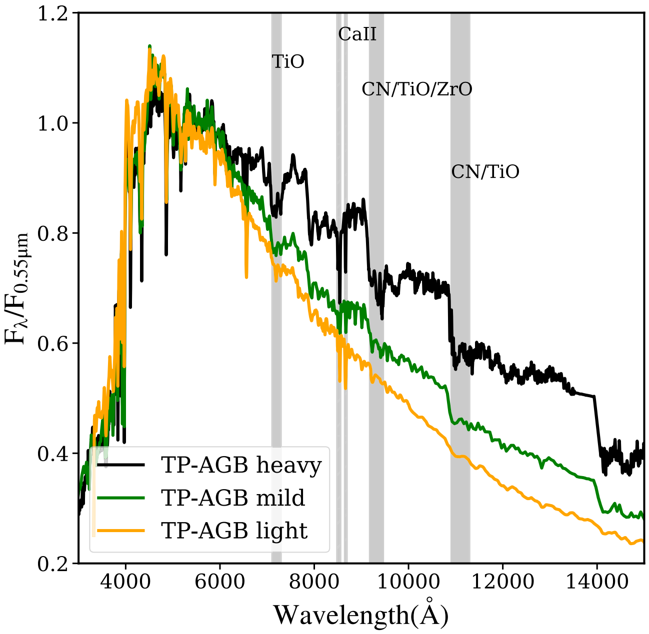

Figure 1. The SED of TP-AGB heavy/mild/light models, normalized at 0.55 μm (with a single burst stellar population of 1 Gyr and solar metallicity). The TP-AGB light model has been smoothed to match the spectral resolution of TP-AGB heavy and TP-AGB mild. There are more cool stars and carbon stars observed in the TP-AGB heavy model compared with the TP-AGB light model, which results in higher luminosity and more molecular features in the NIR (marked with vertical lines). Molecular features found in TP-AGB stars are highlighted with gray shaded regions: 0.71–0.73 μm for the TiO feature, 0.917–0.947 μm for the TiO/ZrO/CN mixture feature and 1.09–1.13 μm for the CN/TiO feature. We also mark 0.8476–0.8564 μm and 0.864–0.87 μm for the CaT feature which is not a TP-AGB sensitive feature with a gray shaded area.

Noël et al. (2013) and Capozzi et al. (2016), the TP-AGB mild model was created to match the colors (especially $V-K$) of the MC star clusters versus cluster age (as displayed in Figure 3 of Noël et al. 2013). The TP-AGB mild model has a shift in the onset age of TP-AGB stars of 300 Myr (with a later onset) and a reduced component of TP-AGB fuel consumption when compared to the TP-AGB heavy model. As an illustration, we plot three sets of model SEDs with the normalized flux of a 1 Gyr old galaxy in Figure 1. The models vary significantly in NIR due to the different contributions of TP-AGB stars. Additionally, specific molecular features (e.g., TiO, CN and ZrO) that trace TP-AGB stars are visible even at low spectral resolution.

The TP-AGB calibration using the MCs (Frogel et al. 1990) is thought to overestimate the contributions of TP-AGB stars in galaxies. The overestimation is due to the narrow age and metallicity span, mainly covering the post-starburst (PSB) phase, of the few massive star clusters in the MC. With the need to move beyond the MC clusters (see Figure 4 in Marigo 2015), a broader age–metallicity parameter space for characterizing the contribution of these stars needs to be covered, e.g., with the Panchromatic Hubble Andromeda Treasury (PHAT) survey (Dalcanton et al. 2012; Johnson et al. 2012) and the ACS Nearby Galaxy Survey Treasury (ANGST) survey (Dalcanton et al. 2009).

Recent studies that attempted to observationally constrain the contribution of TP-AGB stars by fitting SEDs of various galaxy types at different redshifts (Kriek et al. 2010; Zibetti et al. 2012; Riffel et al. 2015; Capozzi et al. 2016; Alatalo et al. 2017; Baldwin et al. 2018; Dahmer-Hahn et al. 2018) have yielded conflicting results. Through low-resolution ($R\sim300$–350), high signal-to-noise ratio (S/N) ground-based NIR spectroscopy of 16 z $\sim$ 0.2 PSB galaxies, Zibetti et al. (2012) concluded that the TP-AGB heavy model is disfavored. However, Riffel et al. (2015) reported strong evidence of TP-AGB stellar features with Gemini Near-Infrared Spectrograph (GNIRS) moderate resolution ($R\sim1200$) spectroscopy of 12 nearby spiral galaxies. These spectra reveal the faint cyanide CN and C_2 features that were not observable in Zibetti et al. (2012). Finally, through multi-band photometric fitting of 51 high-z ($z=1.3$–2.7) galaxies with different SPS models, Capozzi et al. (2016) concluded that TP-AGB heavy models are favored. Baldwin et al. (2018) observed a sample of 12 nearby early-type galaxies with a broad age range to determine the impact of age and star formation history (SFH) on their NIR spectra. They argued that the choice of the fitting process and quality of NIR stellar spectral libraries used in SPS fitting played a larger role than the inclusion of TP-AGB stars in stellar population models. Both TP-AGB heavy and TP-AGB light models provided similar quality of fits in their spectroscopic observations, leading to their conclusion that these stars were of less importance than originally thought. Dahmer-Hahn et al. (2018) fit five sets of evolutionary population synthesis models to six early-type galaxies and one spiral galaxy, and they conclude a stellar library with a higher spectral resolution is essential for improving the fitting result. Under low spectral resolution spectral synthesis, where results are more linked to model libraries than the object properties, the Bruzual & Charlot (Bruzual & Charlot 2003) model displays trends toward younger stellar populations, and Maraston (2005) finds more contributions from intermediate-age populations. However, with high-resolution spectral synthesis, different models produce more consistent results, and the result between optical and NIR agrees much better. None of these works used the combination of multi-band photometry and NIR spectroscopy to constrain the overall importance of these stars.

To address the shortcomings of previous works, we construct one of the largest samples of PSBs for studying the impact of TP-AGB stars. PSB galaxies have a preponderance of intermediate-age (0.1–3 Gyr) stellar populations and no ongoing star formation. Therefore, they are the "sweet spot" for detecting and measuring the contribution of TP-AGB stars, as they span the age range during which TP-AGB contributions are expected to peak. Using a consistent data source, the

3D-HST survey (Brammer et al. 2012; Skelton et al. 2014), we fit stellar population models to both Hubble Space Telescope (HST) NIR slitless grism spectra and ground- and space-based photometry in order to take advantage of both the broad shape of the galaxy SED, as well as TP-AGB sensitive molecular features accessible in the grism spectra.

The structure of this paper is as follows: in Section 2, we describe the 3D-HST data and our PSB sample selection from the 3D-HST survey and ancillary photometric surveys. In Section 3, we outline the SPS model fitting procedures. In Section 4, we describe the stellar population fitting results of these PSB galaxies, our results in comparison with previous studies and the difference in the physical properties of the TP-AGB heavy sources compared to the TP-AGB light sources. In Section 5, we discuss the implications of our results in the context of relevant findings from the literature. In Section 6, we present our conclusions and the summary of this study. In this work, we use Wilkinson Microwave Anisotropy Probe (WMAP) 9 cosmology (Hinshaw et al. 2013), AB magnitudes (Oke & Gunn 1983), and assume a Kroupa (2001) IMF.

2. Data and Sample

We select PSB galaxies from the 3D-HST survey (Brammer et al. 2012; Skelton et al. 2014), which provides an extensive photometric catalog for galaxies detected in the observed fields along with associated slitless grism spectra. The data and selection criteria are discussed in Sections 2.1 and 2.2 respectively.

2.1. Overview of 3D-HST Data

The 3D-HST survey provides data products in the five CANDELS fields (AEGIS, COSMOS, GOODS-N, GOODS-S and UKIDSS-UDS). The survey obtained WFC3 G141 grism spectroscopy (Brammer et al. 2012; Momcheva et al. 2016), along with WFC3 H_{140} imaging, parallel ACS G800L spectroscopy and parallel I_{814} imaging. The 3D-HST WFC3 G141 grism covers the wavelength range from 1.075 to 1.7 μm, and the peak transmission is 48% at 1.45 μm. The G141 grism dispersion is 46.5 Å per pixel in the primary first spectral order with a spectral resolution of $R \sim 130$ at $1.4\,\mu$m. The photometry includes reduced WFC3 F125W, F140W and F160W image mosaics of all five CANDELS/3D-HST fields, and multi-wavelength photometry from different surveys (see Skelton et al. 2014 for a full description). Galactic extinction correction (Schlafly & Finkbeiner 2011) at the center of the field is applied to the photometry in that field. We use these data products (v4.1.5 for grism spectra and v4.1 for photometry) from the 3D-HST survey for the spectro-photometric fitting. We do recognize that AGB stars are abundant in dust which emits in the mid-infrared (MIR), however, they are not included in this work for two reasons: (1) the relatively larger photometric error compared with other photometric data points, and (2) the main goal for this work is to check the different levels of TP-AGB contributions mainly in the optical and NIR covered by the slitless grism spectra.

The redshift of each galaxy is determined with the "best redshift" parameter as defined in the 3D-HST catalog. The "best redshift" parameter provides the most accurate redshift across the available measurements (i.e., spectroscopic, grism, and photometric redshifts). For our work, we consider the error of the grism redshift to be comparable with that of typical high-quality broad-band photometry: $\sigma_z \approx 0.0034 \times (1 + z)$. In our sample, 151 sources have ground-based spectroscopic redshifts, 59 sources have grism spectroscopic redshifts and 14 sources have photometric redshifts only.

For the photometry, we use the photometric catalog of the 3D-HST survey (Skelton et al. 2014), where all fluxes are normalized to an AB zero-point of 25, such that: magAB = 25.0–2.5 × $\log_{10}$(flux). The rest frame color and photometry are calculated with the EAZY code (Brammer et al. 2008). The fitting is run by fixing the redshift to be the photometric redshift and the rest frame photometry is calculated with the best fit template in the observed filter.

2.2. Sample Selection

Our goal is to select PSB galaxies that have sufficiently high S/N grism spectra that capture NIR molecular features, in order to characterize the contribution of TP-AGB stars in their stellar populations. The sample selection criteria are as follows:

(1) We select green valley galaxies with rest frame $u - r$ color (u and r refer to the apparent magnitudes). The initial $u - r$ color cut ($0.9 \leqslant u - r \leqslant 2.5$) should include as many green valley galaxies as possible and avoid contamination from the red sequence. Our final selected sample has a $u - r$ distribution from 1.76 to 2.49 as displayed in the left panel of Figure 2. This final distribution is in agreement with two reference green-valley galaxies' $u - r$ color distribution. The first one is the green-valley galaxies from the Galaxy Zoo project in Figure 2 of Schawinski et al. (2014), where $1.4 < u - r$ (dust corrected) <2.8 spans the stellar mass range from $8.8 < \log_{10}(M/M_{\odot}) < 12$. The second one is based on 300,000 low-z face-on galaxies; Jin et al. (2014) give a more quantitative relation about the $u - r$ color that the center of the green valley galaxies in the local Universe should follow, $(u - r)_{0.1} = -0.121 M_{r,0.1} - 0.061$ (the subscript 0.1 signifies the $u - r$ color at $z = 0.1$). With the M_r range ($-16 < M_r < -24$) of our sources from the completeness check, this gives a rough color range from $1.87 < u - r < 2.84$ for the center color of green valley galaxies at that r-band brightness. To ensure completeness, we discard galaxies fainter than the limiting magnitude (typically with absolute magnitude $M_r = -16$ mag).

(2) We also require $J_{\rm obs} < 21.7$ mag. The purpose of this initial $J_{\rm obs}$ band magnitude cut is to ensure enough S/N for detecting NIR molecular features. We compute the J-band

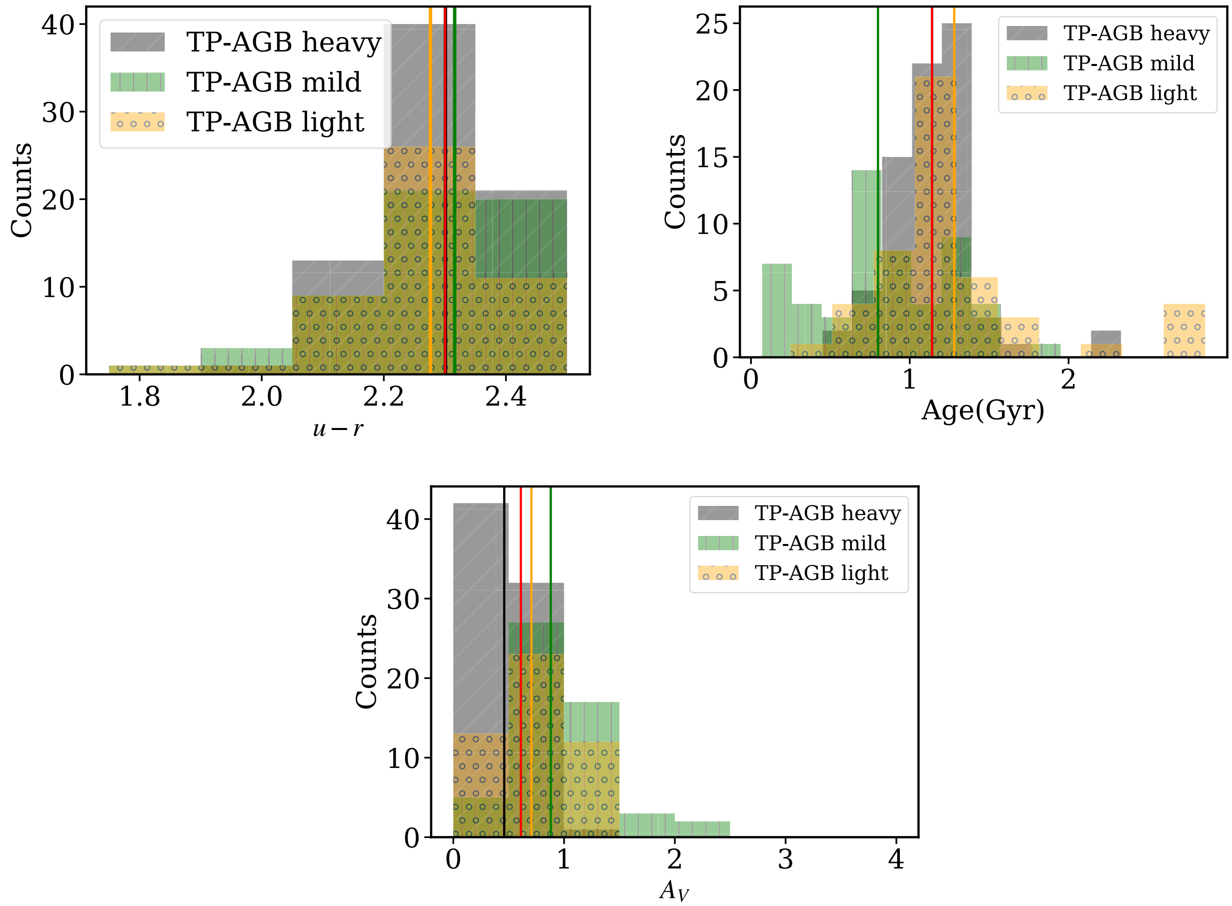

Figure 2. The distribution of $u-r$ color (top-left panel), age (top-middle panel) and $A_{\rm V}$ (bottom panel) for the selected PSB galaxies. The vertical lines mark the median values of three subgroups. The red vertical line signifies the median value for the whole sample.

magnitudes with the observed-frame photometry catalog (Skelton et al. 2014). The 3D-HST catalog draws from WIRDS (Bielby et al. 2012) for the AEGIS field, UltraVISTA (McCracken et al. 2012) for the COSMOS field, MODS (Kajisawa et al. 2011) for the GOODS-N field, ESO/GOODSVLT/ISAAC (Retzlaff et al. 2010) for the GOODS-S field and UKIDSS (Almaini et al. 2007) for the UDS field, with a depth of at least 23.8 mag in AB magnitude.

(3) We remove stars identified with `class_star` > 0.8 or `use_phot` = 0. As described in Skelton et al. (2014), `use_phot` = 1 is equivalent to `nexp_f160w > 2` (F160W exposures over two times), `nexp_f125w > 2` (F125W exposures over two times), `near_star = 0` (not close to a star) and `star_flag = 0` (for galaxies). The `use_phot = 0` flag removes 18 grism spectra from the selected sample. We will use the same S/N threshold (flux/flux_err > 3) for the following photometric fits as discussed in Section 3.2 from the 3D-HST catalog.

(4) We remove low-z targets ($z_{\rm best} < 0.2$) and the final redshift range is $0.2 \leqslant z_{\rm best} \leqslant 0.7$. Because these five fields are deep fields, to avoid the low-mass dwarf galaxies at low redshift, we select the galaxies with a lower limit of $z \geqslant 0.2$. The higher end ($z \leqslant 0.7$) ensures NIR grism spectra cover TP-AGB sensitive features at 0.93 μm (a mixture of TiO/ZrO/CN).

(5) We select galaxies located in the quiescent region in the rest frame *UVJ* diagram, as defined in Whitaker et al. (2011) to ensure they are not star-forming. We remove galaxies with significant ongoing star formation from the selected samples in the *UVJ* diagram in Figure 3 (only keep the galaxies in the upper left part of the *UVJ* diagram, the quiescent region). The rest-frame photometry we use is provided in the *3D-HST* catalog (Skelton et al. 2014) obtained using EAZY templates (Brammer et al. 2008) and the best fitting redshift for each galaxy. The *UVJ* diagram is plotted with the rest frame $U-V$ and $V-J$ colors, and the quiescent galaxies are located in the

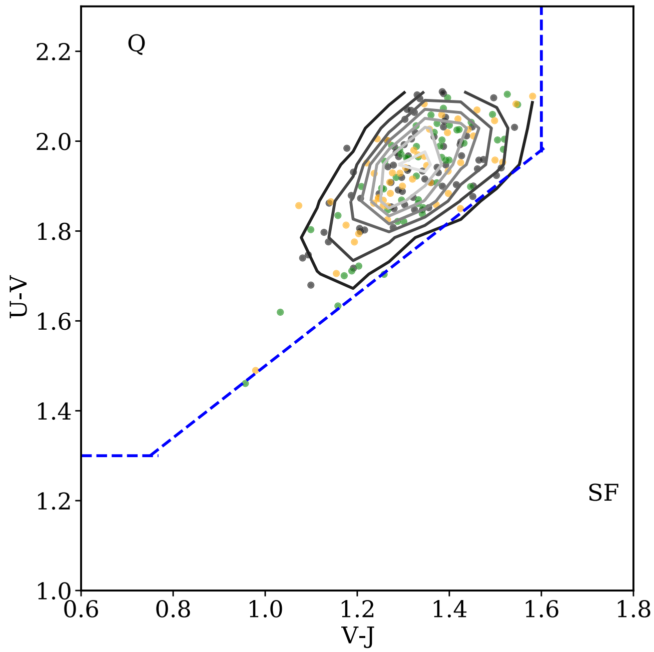

Figure 3. The *UVJ* diagram of the selected galaxies. The black, green and orange circles mark the sources that are best fit with the TP-AGB heavy/mild/light models separately as discussed in Section 3.

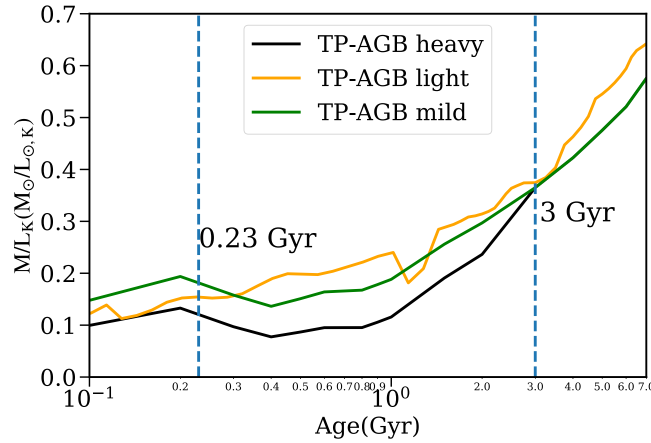

Figure 4. The evolution of M/L_K for the TP-AGB heavy model (Maraston 2005), TP-AGB mild model (Noël et al. 2013), and TP-AGB light model (Bruzual & Charlot 2003). Within the age range from 0.23 to 3 Gyr , the TP-AGB light model has a higher mass-to-light ratio than the TP-AGB heavy model.

Table 1
Summary of the PSB Samples

Field	Number of Grism Spectra	Number of Galaxies
AEGIS	25	21
COSMOS	45	41
GOODS-N	31	25
GOODS-S	69	44
UDS	54	46
Total	224	177

following region according to Whitaker et al. (2011)

$$(U - V) > 1.3,$$
$$(V - J) < 1.6,$$
$$(U - V) > 0.875 \times (V - J) + 0.6. \quad (1)$$

(6) Lastly, we carry out a data quality cut by investigating the S/N of the spectra and photometry for our sources. We define the typical S/N of the grism spectrum to be $\mathrm{S/N} = \mathrm{median}(\frac{\mathrm{Flux}}{\mathrm{Flux_{err}}})$. We require the median S/N of each grism spectrum to be larger than 25 after discarding the data points with $\mathrm{S/N} < 3$ to include a source in our sample. For our analysis, we only use photometric data points with (flux/flux_err) > 3. The photometric errors provided in the catalog do not include shot noise. To account for this, we add the error in quadrature (10% for the ground-based data and 3% for the space-based data) following Iyer & Gawiser (2017). If two photometric data points covering the same wavelength range of the same source are inconsistent with each other, we select the most reliable one, i.e., HST over ground-based, broad-band over medium-band.

This selection yields 177 galaxies in total for the five fields, with 224 grism spectra (some galaxies have duplicated grism measurements from the different pointings). We list the number of PSBs and grism spectra in each field in Table 1. The overall goal is to select PSB galaxies aged 0.1–3 Gyr after the most recent starburst. Furthermore, within this age interval, the model predictions of M/L_K from TP-AGB differ the most from those of TP-AGB light as illustrated in Figure 4, and can yield substantially different infrared (IR) stellar mass estimates.

3. SED Fitting

In this section, we describe the method used to fit stellar population models and show the results for the PSB sample. A flowchart summarizing the fitting procedures is illustrated in Figure 5 and described in further detail below. For the purpose of spectro-photometric fitting, we normalize the observed grism spectra, the model spectra, and all the photometric points with the photometric data point that is closest to 0.55 μm in the rest frame for model fitting. F_ν is converted to F_λ.

Our primary goal is to derive the stellar population parameters (age and A_V) as well as constrain the importance of TP-AGB stars from the fitting. Given that we do not have additional metallicity measurements, we assume solar metallicity for our models.

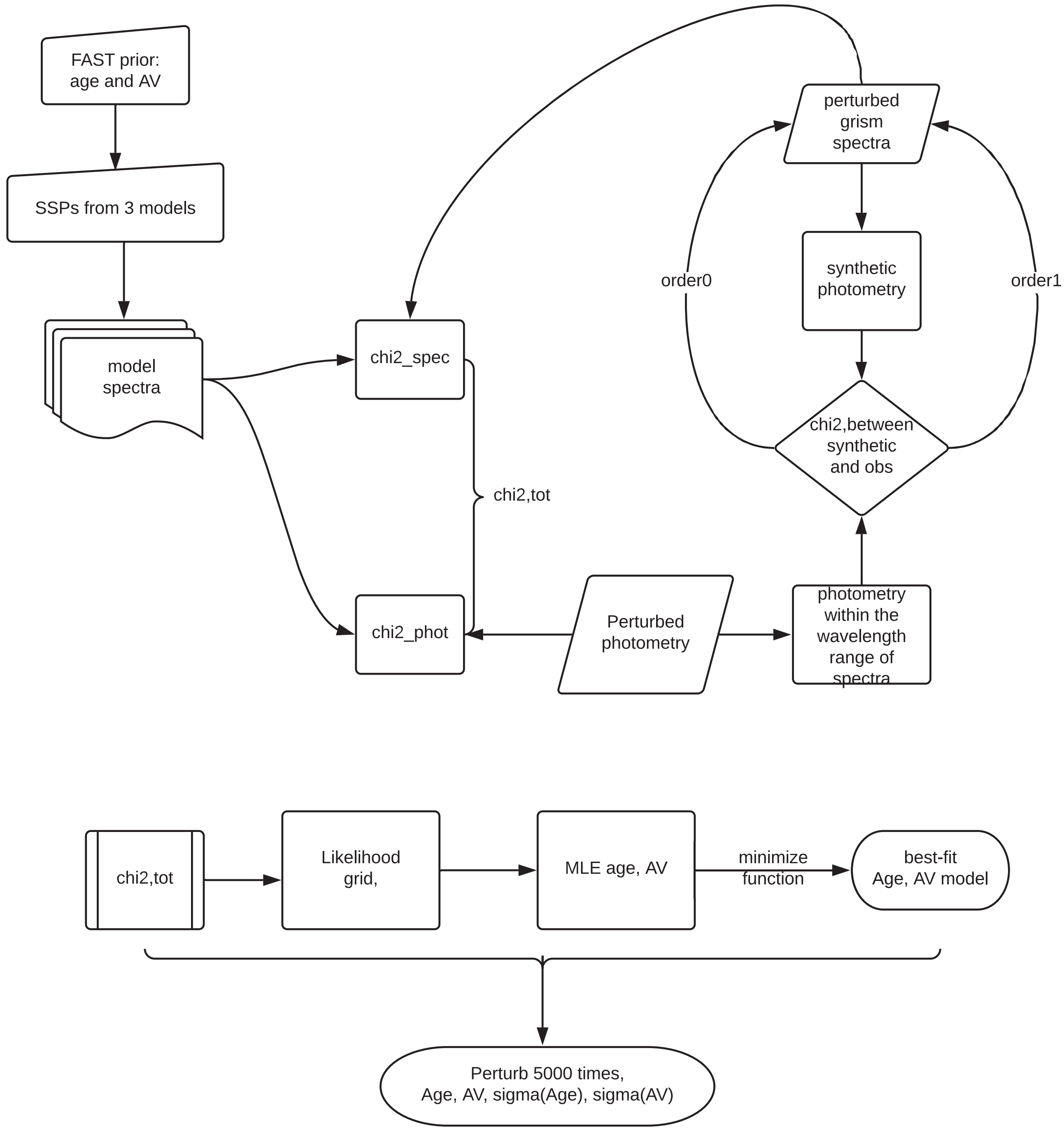

Figure 5. Flow chart depicting the SPS fitting procedure.

3.1. Smoothing the Model Spectra

As listed in Table 2, the spectral resolutions of the three sets of models considered (TP-AGB heavy/TP-AGB mild/TP-AGB light) vary and are higher than the spectral resolution of the grism spectra. We manually determine the full width at half maximum (FWHM) of the model spectra by fitting different Gaussian kernels to the absorption features, typically the Balmer absorption lines for ultraviolet (UV) and optical and Paschen absorption lines for NIR. We note that for the Gaussian kernel we use $\Delta\lambda = 2.355\sigma$. We find the kernel with the minimum residual to be the FWHM and list the values in Table 2, FWHM column. Prior to fitting model spectra to the

Table 2
Comparison of the Parameters in Each SPS Model

Model	IMF	Age (Gyr)	Age Grids	UV and Optical			NIR		
				Library	FWHM	Sampling Interval	Library	FWHM	Sampling Interval
TP-AGB heavy	Kroupa	2.18×10^{-3}–15[1]	46	BaSeL2.2	20 Å	5 Å	BaSeL2.2	50 Å	5 Å
TP-AGB mild	Kroupa	10^{-6}–15[1]	67	BaSeL2.2	20 Å	10 Å (1000 Å –2895 Å) 20 Å (2910 Å – 9990 Å)	BaSeL2.2	50 Å	50 Å (10025 Å –15975 Å) 100 Å (16050 Å –24950 Å)
TP-AGB light	Kroupa	0–20[1]	221	STELIB	3 Å	8.3 Å (1500–2900 Å) 16.7 Å (2900–3322 Å) 1 Å (3322–8750 Å)	BaSeL3.1	50 Å	16.7 Å (8750–10000 Å) 33.3 Å (10000–16000 Å)

observed ones, we smooth the model spectra to match the spectral resolutions of the observed ones.

For each spectrum, the following steps are taken to match the spectral resolution. The model spectra are smoothed in the observed frame with a Gaussian kernel whose size is calculated using Equation (2). The grism spectral resolution is 46.5 Å pix^{-1} as specified in the instrument handbook (Dressel 2012). However, according to Momcheva et al. (2016), the pixels in both the direct image and slitless grism spectroscopy are interlaced, thus the $\Delta\lambda$ is 46.5/2 [Å pix^{-1}]. Furthermore, to account for morphological broadening (van Dokkum et al. 2011), we multiply the smoothing kernel with the source size as measured from the F140W filter. The sizes are provided by the `FLUX_RADIUS` parameter in the 3D-HST photometric catalog, which specifies the circular aperture radius that encloses 50% of the total flux. Finally, the wavelength grids of the smoothed model spectra are re-sampled to match that of the observed spectrum and shifted back to the rest frame.[4]

$$\sigma_{\mathrm{smooth}} = \sqrt{\sigma^2_{\mathrm{grism}} - \sigma^2_{\mathrm{model}}} = \frac{\sqrt{(\mathrm{FLUX\_RADIUS[pix]} \times 46.5\,/\,2[\text{Å pix}^{-1}])^2 - (\sigma_{\mathrm{model}}[\text{Å}] \times (1+z))^2}}{\mathrm{sampling\ interval} \times (1+\mathrm{z})[\text{Å pix}^{-1}]}. \tag{2}$$

3.2. Spectro-photometric SED Fitting

We use the SPS fitting with models with different treatments of TP-AGB stars (Bruzual & Charlot 2003; Maraston 2005, 2012) to determine their importance in our sample. We fit the observed photometry and spectra of the PSB sample with the following model assumptions: solar metallicity, single burst stellar population, a Kroupa (2001) IMF, no nebular emission lines, and the Calzetti (2001) dust attenuation law with $R_V = 4.05$. First, we create a wavelength-dependent mask (the wavelength range that we use is from 11 407.53 to 16 428.61 Å) in the observed frame according to the grism sensitivity curve. The sensitivity marks the conversion from electron counts to flux densities and depends on the grism throughput and the quantum efficiency of the detector. We discard the edges of the spectra where the sensitivity is low and is most impacted by calibration errors, as plotted in Figure 6. Within the unmasked wavelength range, there are still some sources where the flux error is quite large. We remove these targets from the overall source list due to min(flux/flux_err) < 0 and visually verify the quality of all remaining grism spectra.

Second, we remove the non-detections of photometric data points, which are marked with negative photometric flux and/or S/N = 1 in the photometric catalog.

[4] Only the models within the age range between 0–13 Gyr are actually employed in the fitting procedure of this work.

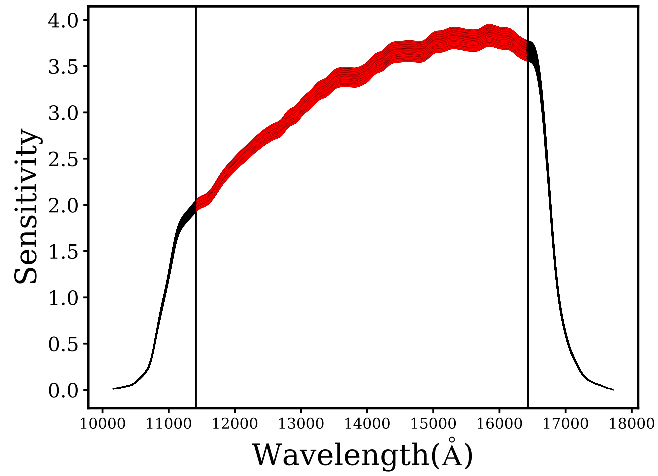

Figure 6. The sensitivity-wavelength plot for 45 grism spectra in this work from the COSMOS field. (Due to the slight differences between the different spectra, the sensitivity curves are not the same for all the spectra.) We mark the edge of the wavelengths of interest with black lines and the regions of interest on the sensitivity curve are marked red from 11407.53 to 16428.61 Å. We choose this wavelength range because, in this region, the sensitivity does not vary too much with wavelength.

Third, we scale the grism spectra to the photometry to account for the aperture differences. The photometry is extracted within an aperture defined with `FLUX_RADIUS`, while the grism spectroscopy is extracted within the spatial extent three times the `SExtractor FLUX_RADIUS` (at least 26 interlaced pixels). Only the photometric bands that are fully covered by the grism spectra are considered when calculating the re-scaling factor. The number of photometric points covering the same wavelength range as the grism spectra ranges from 1 to 4. For the re-scaling, we use either a zeroth-order or a first-order polynomial, whichever returns the minimum χ^2_ν for the whole spectro-photometric fit. Higher order corrections are not necessary for the sources where only fewer than one or two photometric points fully overlap with the grism wavelength coverage; 177 of the sources use a zeroth order re-scaling, and the rest of the sources use a first order re-scaling.

As priors for the SED fitting, we use the age and A_{V} estimated from the FAST code (Kriek et al. 2009), which is provided by the 3D-HST catalog (see Figure 5). The best fitting FAST parameters are determined using the Bruzual & Charlot (2003) stellar population synthesis library with the Chabrier (2003) IMF, solar metallicity, exponentially declining SFH, and the Calzetti et al. (2000) extinction law.

3.2.1. Evaluating the Goodness of Fit

We evaluate the goodness of fit for each of the three sets of models by computing the χ^2_ν of the spectra and the photometry. We devise goodness of fit that combines photometry and spectroscopy in a self-consistent way. The first step of this process is to compute independent χ^2 for photometry $\chi^2_{\rm phot}$ and spectroscopy $\chi^2_{\rm spec}$.

$\chi^2_{\nu,\rm spec}$ is computed in the rest frame as

$$\chi^2_{\nu,\rm spec} = \frac{1}{n-2}\sum_{i=1}^{n}\frac{(F_{\lambda,{\rm data},i} - F_{\lambda,{\rm model},i})^2}{\sigma^2_{\lambda,{\rm data},i}}, \tag{3}$$

where n is the number of spectroscopic data points, $F_{\lambda,{\rm data},i}$ is the observed flux of the grism spectra and $\sigma^2_{\lambda,{\rm data},i}$ is the observed variance. Here we consider the degrees of freedom to be $n-2$, where n is the number of spectroscopic data points, and the number of parameters to be 2 (age, $A_{\rm V}$). The $F_{\lambda,\rm model}$ is obtained by interpolating the model spectra with the wavelength grid of the grism spectra.

$\chi^2_{\nu,\rm phot}$ is computed as follows. For a given parameter set (age, $A_{\rm V}$) of a specific model, we obtain the model photometry by shifting the model spectra to the rest frame and multiplying them with the filter transmission curves

$$F_{\lambda,\rm phot,model} = \frac{\sum_{i=1}^{m}{\rm transmission_i} \times {\rm F}_{\lambda,{\rm model},i}}{\sum_{i=1}^{m}{\rm transmission_i}}, \tag{4}$$

where m represents the number of wavelength elements that fall within the transmission curve of a given filter. We calculate $\chi^2_{\nu,\rm phot}$ as follows

$$\chi^2_{\nu,\rm phot} = \frac{1}{{\rm n}-2}\sum_{i=1}^{n}\frac{(F_{\lambda,{\rm phot,data},i} - F_{\lambda,{\rm phot,model},i})^2}{\sigma^2_{\lambda,{\rm phot,data},i}}, \tag{5}$$

where $F_{\lambda,\rm phot,data}$ and $\sigma_{\lambda,\rm phot,data}$ are the observed photometric flux and the observed photometric flux error from the catalog as described in Section 2.2.

Considering the different levels of error in the photometry and grism spectra, we weigh both χ^2 contributions differently by calculating their relative weights in the total χ^2 in order to ensure $\chi^2_{\nu,\rm tot} \sim 1$. The goodness of fit of the spectro-photometric SED fitting is evaluated by combining the two parts using the weighted χ^2_ν with the following equation

$$\chi^2_{\nu,\rm tot} = 0.5 \times ({\rm weight1} \times \chi^2_{\nu,\rm spec} + {\rm weight2} \times \chi^2_{\nu,\rm phot}). \tag{6}$$

We go through an initial round of fitting where both weights are set to be 1. We determine the median value of the two distributions of $\chi^2_{\nu,\rm spec}$ and $\chi^2_{\nu,\rm phot}$ to calculate the weights and check to see if the median $\chi^2_{\nu,\rm tot}$ distribution is centered at 1. We continue with another round of fits with the modified weights $\chi^2_{\nu,\rm tot}$ until the distribution of $\chi^2_{\nu,\rm tot}$ is centered at 1. This method empirically determines the appropriate weighting of the photometric and spectroscopic data in the combined spectro-photometric fit.

During the fitting procedure, we linearly interpolate the spectra as a function of age to find the best fit parameters for each model separately. The interpolation procedure is done by finding the closest age pair from the model age grids given the current input age, and we calculate the model spectra using the following equation

$$F_{\rm model} = \frac{1}{({\rm age_{model2}} - {\rm age_{model1}})}[({\rm age_{model2}} - {\rm age}) \times F_{\rm model1} + ({\rm age} - {\rm age_{model1}}) \times {\rm F_{model2}}]. \tag{7}$$

Here age is the input age, and $\rm age_{model1}$ and $\rm age_{model2}$ are the closest model age grids in which the input age lies. $F_{\rm model1}$ and $F_{\rm model2}$ are the corresponding F_λ from these two models.

We use the minimization function `SLSQP` method (minimize a scalar function of one or more variables using Sequential Least SQuares Programming) from the `scipy.optimize.minimize` package to find the best pair of age and $A_{\rm V}$ for each of the three models. This method minimizes a function with variables subject to bounds, where the age is bound within 0–13 Gyr and $A_{\rm V}$ within 0–4. The model with the smallest $\chi^2_{\nu,\rm tot}$ is identified to be the best fit model. An example SED displaying the spectroscopic (with red lines) and photometric (with red error bars) data for different TP-AGB models is depicted in Figure 7.

To derive the uncertainties of the derived parameter sets, we run Markov Chain Monte Carlo (MCMC) for the full sample with the probability using a likelihood function defined below (Equation (8)) to feed into the ensembler. n is the total number of data points at each wavelength grid for each source, x_1 is the flux of the observed spectra and μ_1 is the flux of the model spectra. The quoted errors are derived from the projections of the 39.3% error region of the two-dimensional (2D) distribution onto the respective axes.

$$\begin{aligned} p_{\rm tot} &= p_1 p_2 \cdots p_n \propto \exp-\frac{1}{2}\frac{(x_1-\mu_1)^2}{\sigma_1^2} \\ &\times \exp-\frac{1}{2}\frac{(x_2-\mu_2)^2}{\sigma_2^2} \cdots \exp-\frac{1}{2}\frac{(x_n-\mu_n)^2}{\sigma_n^2} \\ &= \exp-\frac{1}{2}\sum_{i=1}^{n}\frac{(x_i-\mu_i)^2}{\sigma_i^2}. \end{aligned} \tag{8}$$

An example of the derived parameters is provided in Figure 8.

4. Results

In this section, we present the model fitting results, with the goal to evaluate the contribution of TP-AGB stars in the SEDs of the PSB galaxies, and whether grism spectra provide additional constraints in addition to photometry alone.

4.1. Classification of Best Fit Models

Our SED fitting procedure determines both the best fit age and A_V of a given model as well as which of the three TP-AGB models (Table 3) produces the lowest $\chi^2_{\nu,\rm tot}$. This yields the

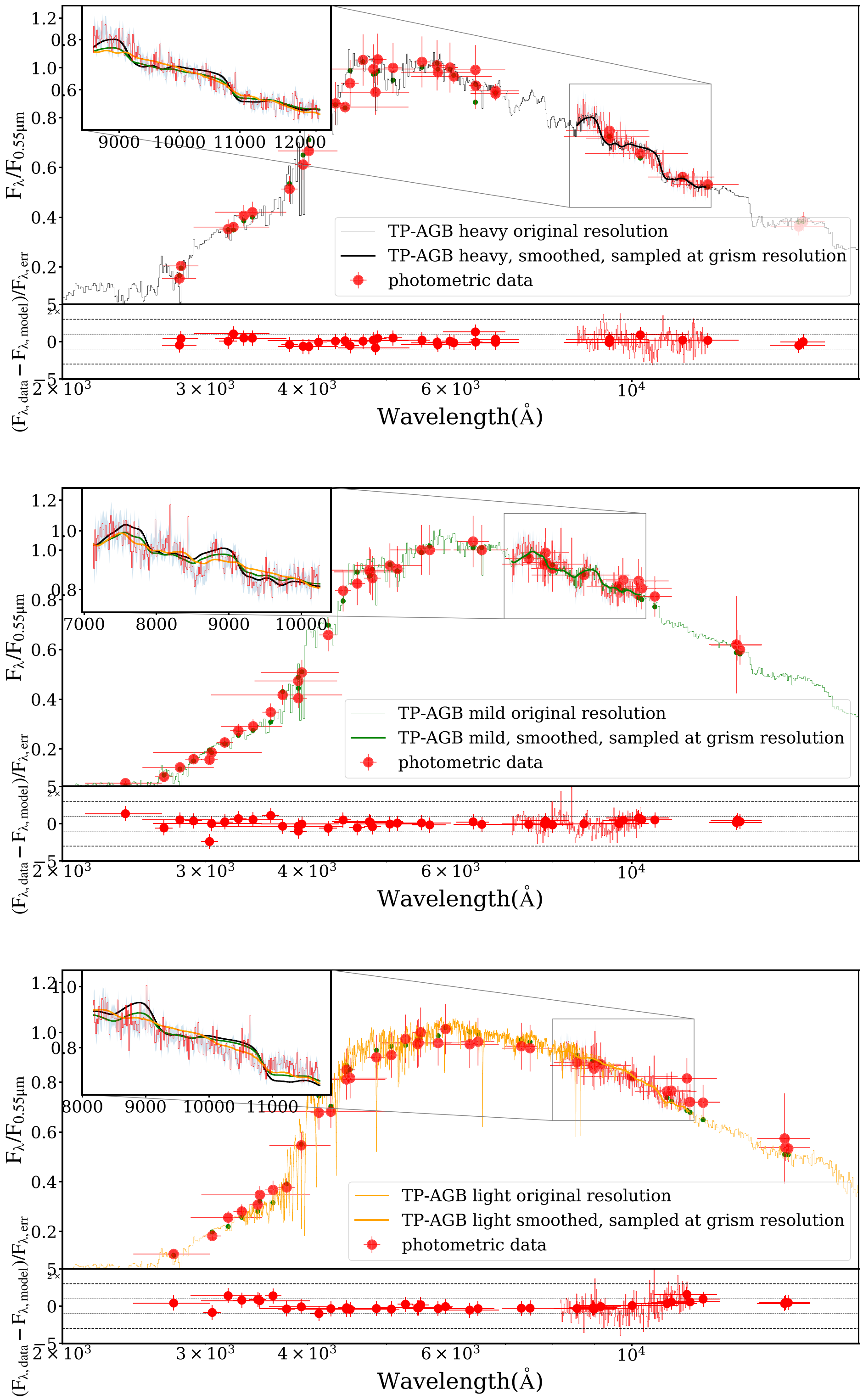

Figure 7. Example of the spectro-photometric fitting result of three galaxies best fit with three respective models: TP-AGB heavy (Maraston 2005) (top), TP-AGB mild (Noël et al. 2013) (middle) and TP-AGB light (Bruzual & Charlot 2003) (bottom). We plot the grism spectra with the red curve. The photometric data points are marked with red circles, where the vertical lines indicate errors and the horizontal lines signify wavelength coverage. We also plot the model with optimized age and A_V applied according to the color scheme in the legend (see Table 2 for details). The inset image displays the zoomed-in region of the grism spectra and the smoothed model spectra. In the lower panel for each subplot, we plot the relative residuals of the photometric data over the best fit model and the relative residuals of the grism spectra over the best fit model. The *y*-axis is in units of standard deviation.

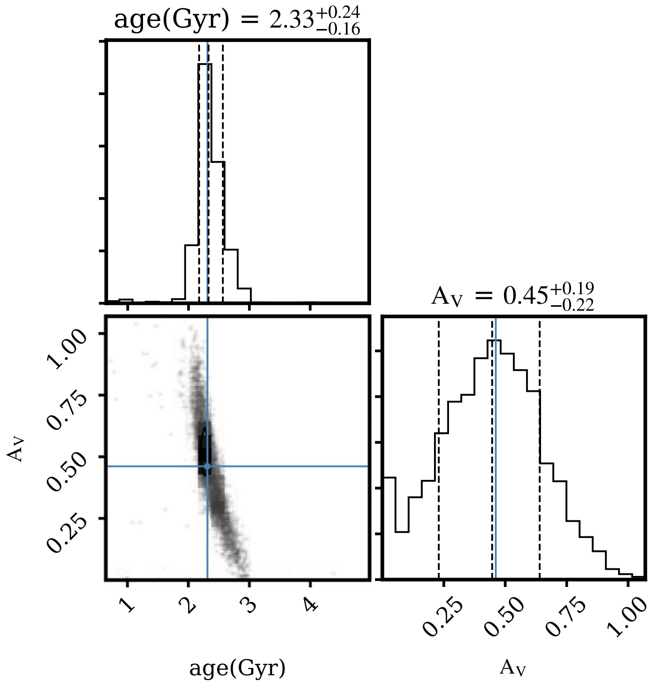

Figure 8. The corner plot of COSMOS-24-10494 fitting with the TP-AGB heavy model. The two fitting parameters are the age (Gyr) of a single stellar population and the dust attenuation A_V. The cross marks the age and A_V of the best fit with the lowest χ^2.

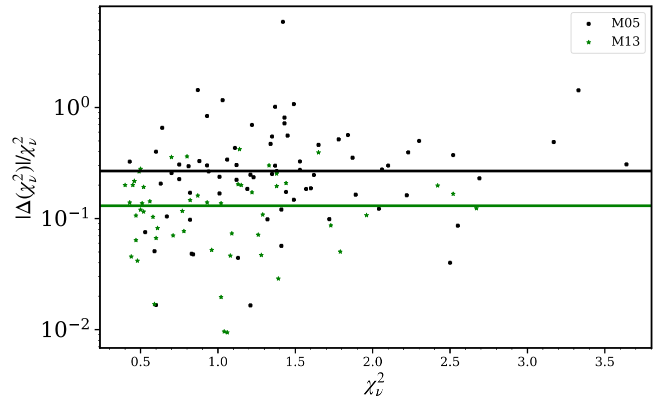

Figure 9. The fractional difference of χ^2_ν for the best fit model and χ^2_ν of the TP-AGB light model (Bruzual & Charlot 2003). The vertical axis shows the fractional difference of χ^2_ν while the horizontal axis displays χ^2_ν from the best fit model.

Table 3
Classification of Best Fit TP-AGB Models

	Heavy	Mild	Light
galaxies	75	54	48
spectra	110	58	56

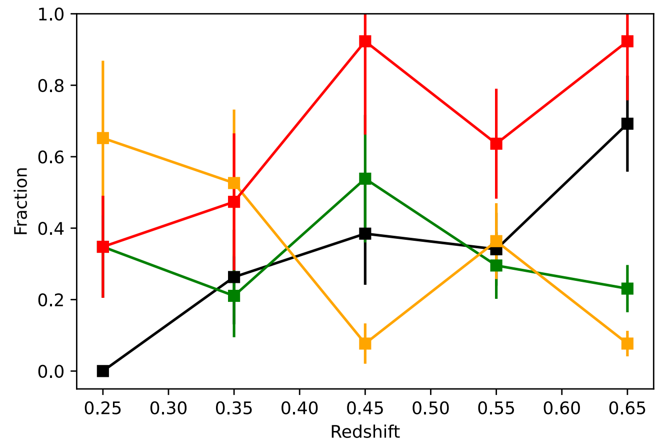

Figure 10. The fraction of galaxies classified as TP-AGB heavy (black), mild (green) and light (yellow) as a function of redshift. The red curve signifies the fraction of TP-AGB heavy and mild galaxies. There is a statistically significant trend observed where there is a greater fraction of TP-AGB heavy systems at higher redshifts and a corresponding inverse trend for TP-AGB light systems.

following result: 75, 54 and 48 galaxies are best fit by TP-AGB heavy, mild and light models, respectively. This means that 72.9% of the PSB galaxies at $0.2 \leqslant z \leqslant 0.7$ show clear signatures of TP-AGB stars as they are best fit by either TP-AGB heavy or mild models rather than TP-AGB light models.

We confirm the robustness of this result by comparing the fractional difference in $\chi^2_{\nu,\rm tot}$ between the best fit model and the TP-AGB light model, as affirmed in Figure 9. Over 81.3% of the galaxies that are best fit with TP-AGB heavy models have $\Delta\chi^2/\chi^2$ larger than 10%, and over 64.8% of the galaxies that are best fit with the TP-AGB mild models have $\Delta\chi^2/\chi^2$ larger than 10%. This suggests there is a substantial difference in the χ^2 between the TP-AGB light and TP-AGB heavy/mild models.

As another test, we compare the model classifications of 27 galaxies that have multiple observations yielding multiple grism spectra. These galaxies share the same model classification results regardless of the spectra used (20 galaxies with two grism spectra, 1 galaxy with three grism spectra, 1 galaxy with four grism spectra and 4 galaxies with five grism spectra). We tabulate the model classification results in Table 3. We conclude that the TP-AGB heavy model best describes the majority of the PSB galaxies at $0.2 \leqslant z \leqslant 0.7$ selected from the 3D-HST survey.

4.2. Redshift Dependence of Model Classification

Given the relatively broad redshift range of our sample, we examine the dependence of model classification on redshift. We compute the fraction of galaxies classified by each model in

Table 4
K-S Test of TP-AGB Heavy/mild Samples vs. TP-AGB Light Samples

Property	K-S Test Result	p-value
$u-r$	0.14	0.34
age	0.38	5.9e-5
A_V	0.19	0.13

$\Delta z = 0.1$ redshift bins over the $z = 0.2$–0.7 sample range. The errors in the fractions are determined by Poisson statistics. The results are displayed in Figure 10. We observe a redshift dependence in the fraction of TP-AGB heavy and TP-AGB light models. TP-AGB heavy models feature a strong positive trend with redshift whereas light models manifest an inverse correlation. Mild models exhibit no redshift dependence.

This is suggestive of a real physical effect where there is a greater incidence of galaxies that show strong TP-AGB features at higher redshift. However, there are other potential causes of this, which include our assumption of simple stellar populations (SSPs). There is a distinct possibility for the growing dominance of composite stellar populations at lower redshift, which dilutes the TP-AGB features and yields a TP-AGB light classification. We discuss this further in Section 5.

4.3. Comparing TP-AGB Heavy Galaxies with TP-AGB Light Ones

To discern possible differences in the PSB galaxies with strong or weak TP-AGB contributions, we compare their colors, dust attenuation, and ages in Figure 2. Specifically, we rely on the Kolmogorov–Smirnov (K-S) test to verify whether the stellar population parameters ($u - r$ color, age, A_V) are statistically different between the two samples (TP-AGB heavy + mild samples versus TP-AGB light samples). The K-S test values are expressed in Table 4. Adopting a threshold of $p = 0.01$, we cannot reject the null hypothesis that the A_V and $u - r$ color of the TP-AGB heavy/mild sample are statistically similar to those of the TP-AGB-light sample at a probability of 0.13 and 0.34, respectively. On the other hand, we can conclude that the age distribution of the TP-AGB heavy/mild sample is statistically different from the TP-AGB light one. This is not surprising since the TP-AGB features are highly age-sensitive when compared to those in the TP-AGB light models. This statistical test is simply revealing the property of these models.

4.4. The Importance of Including Grism Spectra in the SED Fitting

When grism spectra are included, they are expected to improve constraints on the derived age and A_V from the stellar population fitting result. To determine the value of including

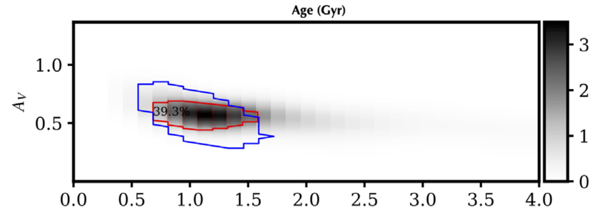

Figure 11. The 1σ error region comparison of the photometry only from photometry-only fitting (blue contour) and spectro-photofitting (red contour); the color-bar indicates the number density in that age (x-axis)–A_V (y-axis) grid.

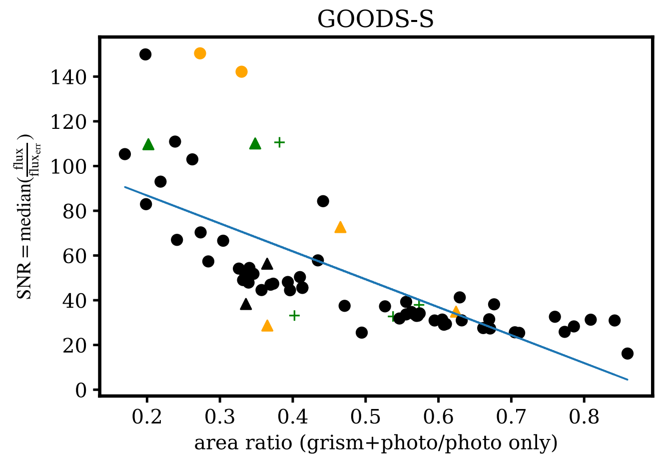

Figure 12. The area ratio of the 1σ error region comparison of the photometry only from photometry-only fitting with the S/N of the grism spectroscopy for GOODS-S sources. The symbol colors represent the fitting result from spectro-photofitting: the black symbols mark the sources that are best fit with TP-AGB heavy model, green crosses signify the sources that are best fit with the TP-AGB mild model and orange triangles indicate the sources that are best fit with the TP-AGB light model. The symbol shapes represent the fitting result from photometry-only fitting, where the circles mark the sources that are best fit with TP-AGB heavy model, crosses signify the sources that are best fit with TP-AGB mild model and triangles indicate the sources that are best fit with the TP-AGB light model. We fit the sources with a line to illustrate the decrease of the area ratio with the increase of S/N.

grism spectra in SED fitting, we measure the improvement in uncertainty estimates with and without the inclusion of grism spectra as follows: (1) We calculate the area that is encircled within the 1σ region of the age–A_V contour, which accounts for 39.3% of the total samples in the 2D distribution. (2) We generate two sets of contour plots: one with photometry only, and one with photometry and the grism spectroscopy, as depicted in Figure 11. (3) We separate the age into 100 bins from 0.1 times the input age to 3 times the input age, and A_V into 40 bins from 0 to 5 times the input A_V at maximum with 4.0, and consider the area from age and A_V bins as the grid. The area is defined by the number of grids encircled within this 1σ contour times the width of the grid defined by the age and the height of the grid defined by A_V.

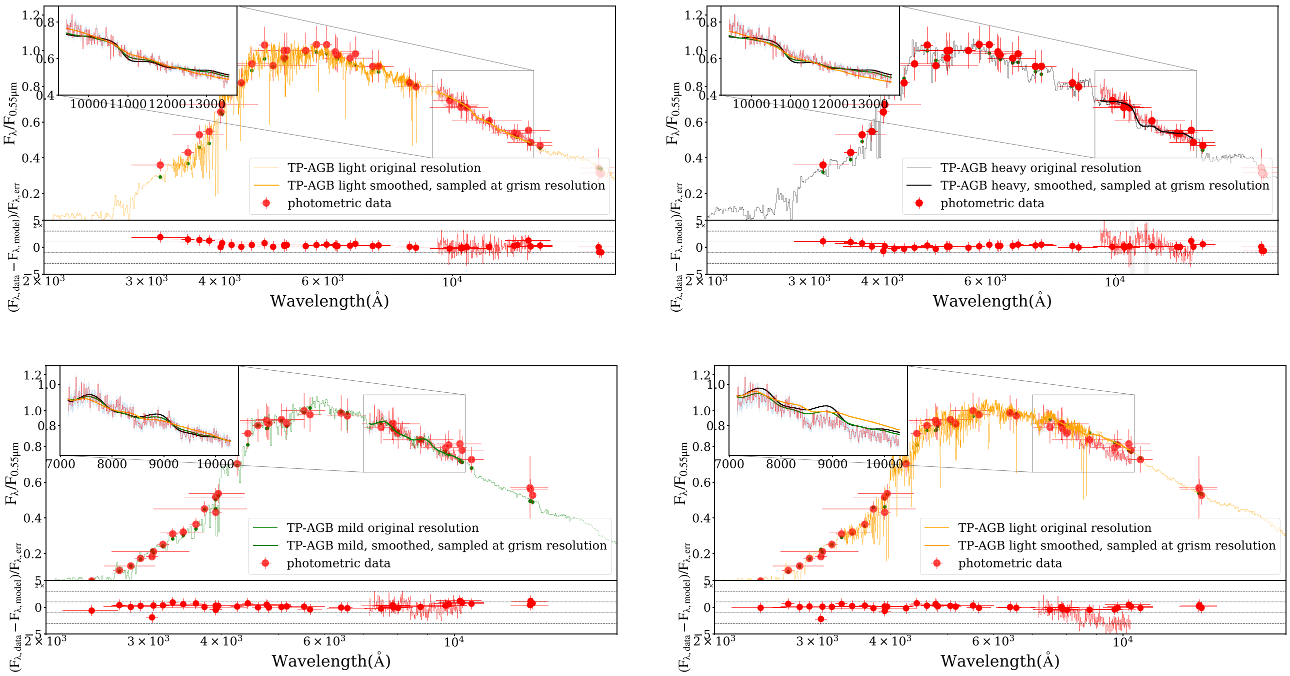

Figure 13. The spectro-photometry fitting result of COSMOS-3-13683 (upper panels) and COSMOS-16-20605 (lower panels). In the left panels, we demonstrate the best fit models with spectro-photometry fitting, while best fit models with photometry-only fitting are shown in the right panels. The residuals of spectra in the left panels are much smaller than those in the right panels.

As expected, the inclusion of the grism spectra in the SED fitting reduces the uncertainties, and the improvement is more significant when the grism spectra have higher S/N. We use the result in the GOODS-S field as an example in Figure 12.

We carry out another test to check if the inclusion of grism spectra helps to determine the best fit model. We run another set of fits by using photometry only, i.e., setting the weight of the grism spectra to zero. Comparing the model classification based on photometry-only versus spectro-photometric fitting, there are 36 sources that are best fit by TP-AGB light models using photometry only but are re-classified to TP-AGB heavy/TP-AGB mild models when grism spectra are included in the fitting. An example of such a galaxy is COSMOS-3-13683 as shown in the upper panel of Figure 13. On the other hand, 25 sources best fit by TP-AGB heavy/TP-AGB mild models when using photometry alone were re-classified to TP-AGB light models when grism spectra were included in the fitting. An example of such a galaxy is COSMOS-16-20605, featured in the lower panel of Figure 13. A visual inspection of the residuals of the spectral fitting confirms that the fits are improved when grism spectra are included. We thus conclude that grism spectra are critical in identifying best fit models.

4.5. Molecular Feature in Grism Spectra

We further quantify the impact of the inclusion of grism spectra on model classification by comparing the stacked spectra. We separate the sample within the age range of 0.5–1.5 Gyr into three best fitting model classifications, i.e., TP-AGB heavy, TP-AGB mild and TP-AGB light. The spectra are normalized at 0.55 μm and shifted to the rest frame, interpolated with a wavelength grid with 1 Å interval, and stacked. A stacked spectrum is obtained by calculating the weighted mean value of the flux values at each wavelength for the sources. The stacked spectra are shown in Figure 14. Molecular features found in TP-AGB stars are marked with the gray shaded regions: 0.71–0.73 μm for the TiO feature, 0.917–0.947 μm for the TiO/ZrO/CN mixture feature and 1.09–1.13 μm for the CN/TiO feature. As expected, TP-AGB heavy stacked spectra display the deepest absorption values at these targeted features, while the TP-AGB mild stacked spectra exhibit slightly shallower absorption features than the TP-AGB heavy stacked spectra but are still deeper than the TP-AGB light model. Furthermore, we re-run the fitting routine to find the best fit model for the three stacked spectra (here we assume the source has a flux radius of 9.46 pixels, the mean radius value), and demonstrate the result in Figure 15, where the spectral difference between the models is significant. Here we consider each stacked spectrum to be a single source to be fed into our fitting routine, where we place full weight onto spectral fitting and no weight on photometry fitting. The $\Delta\lambda$ is 219.9 Å, equivalent to a spectral resolution of about 43.

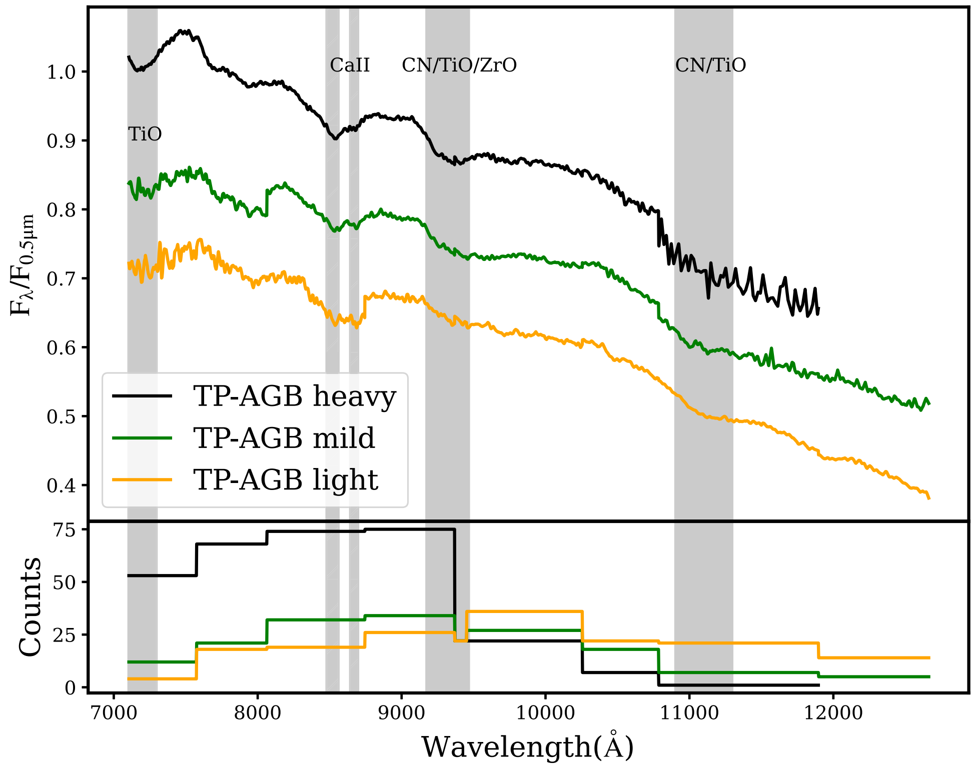

Figure 14. (Top) The stacked grism spectra of the PSB galaxies best fitted by TP-AGB heavy (black curve), TP-AGB mild (green curve) and the TP-AGB light (orange curve) models. Only PSB galaxies within an age range of 0.5–1.5 Gyr are included in the stacks. The gray shaded regions mark the targeted features: TiO at 0.72 μm, CaT, TiO/ZrO/CN at 0.93 μm and CN/TiO at 1.1 μm. (Bottom) The number counts of spectra included in the stacks as a function of wavelength.

Altogether, these results demonstrate that the inclusion of grism spectra indeed improves the accuracy of the model classification and that a majority of the sample of PSB galaxies have a non-negligible contribution from TP-AGB stars in their SEDs.

4.6. Impact of TP-AGB Contribution on Stellar Mass Estimates

In this subsection, we discuss the variations of stellar mass-to-light ratios from different TP-AGB contributions and the corresponding differences in inferred stellar masses when TP-AGB stars are properly accounted for.

4.6.1. Mass-to-light Ratios

We estimate the stellar masses of the galaxies using the mass-to-light ratios, M/L_K, of the respective best fit models (see Figure 4), and the rest frame K-band luminosities. The M/L_K of the TP-AGB heavy model is estimated from the Kroupa IMF. The M/L_K of the TP-AGB mild model is calculated in the following way. The K-band magnitude is extracted from the TP-AGB mild SED convolved with a K-band filter, while the mass of the stellar population is given by the normalized model. The M/L_K of the TP-AGB light models is generated by GALAXEV (Bruzual & Charlot 2003). Between the age range from 0.23 to 3 Gyr (as marked in Figure 4), the M/L_K of TP-AGB heavy models is lower than that of the TP-AGB light models. In particular, at ages of around 1 Gyr when the luminosity of TP-AGB stars is the highest, the M/L_K of the TP-AGB heavy model is almost half the M/L_K of the TP-AGB light model.

4.6.2. Stellar Mass Overestimation

For each galaxy with an identified best fit model and age, we retrieve the M/L_K for a given model and age and obtain the stellar mass by multiplying the M/L_K with the rest frame K-band luminosity from the 3D-HST survey catalog. The resulting stellar masses of the sample are depicted in Figure 16. The difference in the mass distribution of the three subgroups is not significant.

We calculate the mass ratio, defined as the stellar mass estimated from the TP-AGB heavy/mild models over the stellar mass estimated from the TP-AGB light models for the same sources, and display the distribution in Figure 17. For the TP-AGB heavy galaxies, the mean value and median value for the mass ratios are 0.55 and 0.59 respectively. For the TP-AGB

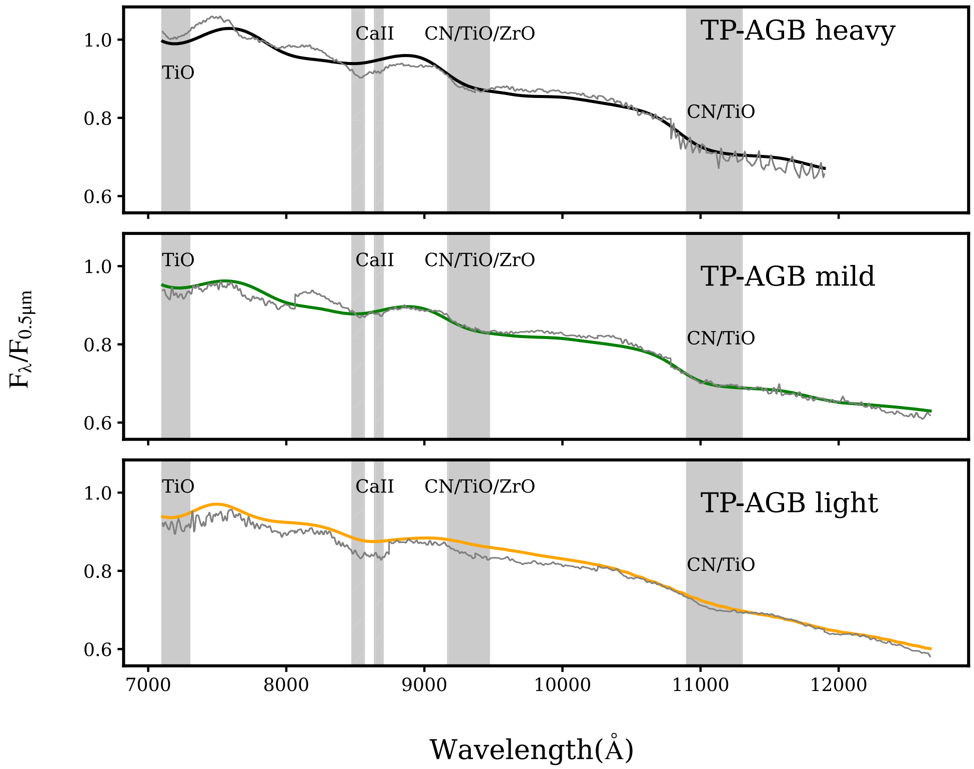

Figure 15. The model fitting result to three stacked spectra. The top, middle and bottom panels are the stacked spectra of the three models and their best fit smoothed model fitting results. We also mark the targeted features with gray shaded regions as in Figure 14. The black line in each panel is the stacked spectrum, and the black/green/orange lines are the smoothed model spectra.

mild galaxies, the mean value and median value for the mass ratios are 0.83 and 0.74 respectively.

We thus conclude that the stellar mass estimates of PSB galaxies can be overestimated if the TP-AGB contribution is neglected in the SED fitting, by up to 0.13–0.23 dex.

5. Discussion

The aim of our work is to shed some light on the debate on the importance of TP-AGB stars using a large sample of PSB galaxies (>150) with high-quality and consistently determined photometry and high S/N NIR slitless grism spectra. Other studies have managed to observationally constrain the contribution of TP-AGB stars by sampling different types of galaxies at different redshifts (Maraston et al. 2006; Kriek et al. 2010; Zibetti et al. 2012; Riffel et al. 2015; Capozzi et al. 2016; Alatalo et al. 2017; Baldwin et al. 2018; Dahmer-Hahn et al. 2018) and have yielded conflicting results. These studies have relied on either photometric or spectroscopic measurements, but not both, over a broad range of redshifts. The combination of photometry and spectroscopy is especially powerful in constraining both the continuum and detecting specific tracer spectra features that are especially evident in the NIR. We discuss how our work relates to previous works.

There have been a number of photometric studies that have yielded conflicting results. Maraston et al. (2006) target a sample of galaxies at $1.4 \leqslant z \leqslant 2.7$ and find TP-AGB heavy models fit better than TP-AGB light ones while providing more consistent photometric redshifts. Kriek et al. (2010) use multi-band photometry of 62 PSB galaxies at $0.7 \leqslant z \leqslant 2.0$, which are then combined to form a single rest frame SED that is then fit. They demonstrate a low contribution from TP-AGB stars to the SED of PSB galaxies. Capozzi et al. (2016) use 51 high-z ($1.3 \leqslant z_{\rm spec} \leqslant 2.7$) galaxies to fit with three sets of models and confirm that without dust attenuation, the TP-AGB heavy model fits better with photometry alone. Though at higher redshift, the Capozzi et al. (2016) sample has similar age and mass distributions and SED wavelength coverage with our sample. They also include samples located in the star-forming region from the NUV-r and r-J plots. They use four different SFHs (SSP, exponentially declining star formation rate (SFR), truncated SFR, and constant SFR), and determine the best fit to be the one with the minimal reduced χ^2. Capozzi et al. (2016), unlike Kriek et al. (2010), obtained spectroscopic redshifts for all of their sample galaxies. They further indicate that photometry-only SED fitting as carried out by Kriek et al. (2010) could be significantly affected by the redshift accuracy

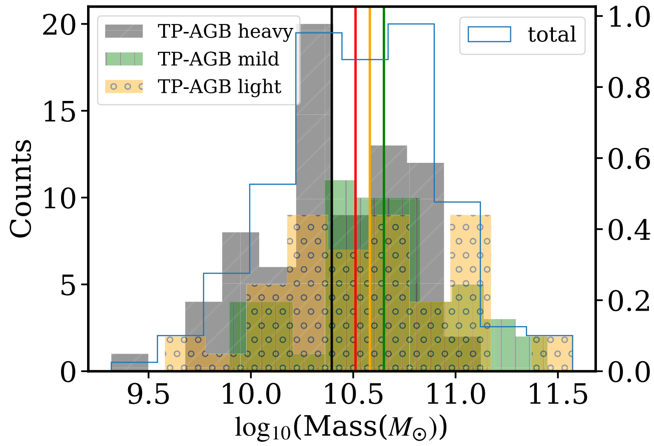

Figure 16. The distribution of the stellar mass estimates of the galaxies for different models. The left vertical axis tells the counts within each mass bin and the right axis corresponds to the probability density: each bin will display the bin's raw count divided by the total number of counts and the bin width. The median values of the three subgroups are signified with black, green and orange vertical lines, respectively. The median value of the full sample is shown by the red vertical line.

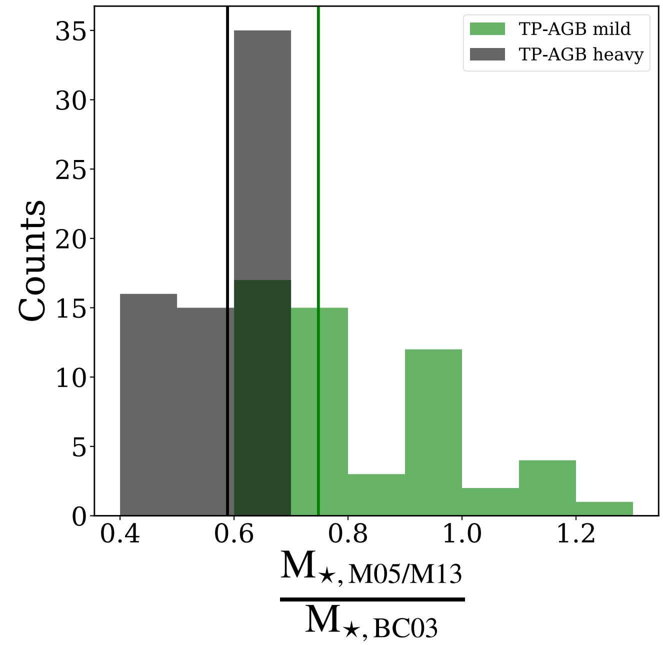

Figure 17. The distribution of the stellar mass ratios of the galaxies with the mass derived from their best fit model over the mass derived from the TP-AGB light model for the sources that are best fit with TP-AGB heavy and TP-AGB mild. The x-axis corresponds to the stellar mass ratio of the TP-AGB heavy/mild galaxies measured from the M/L_K inferred from the corresponding models compared with that calculated from the TP-AGB light models. The median values of the two distributions have been marked with vertical dashed lines.

of the sources because the vast majority of the sources (∼90%) did not have spectroscopic redshifts. However, the Capozzi et al. (2016) work does reveal that photometry-only fitting yields some degeneracy between the dust attenuation and the importance of TP-AGB. This is a fundamental issue in photometry-only SPS fitting.

There were a few spectroscopic studies that also disagree with their conclusions. Through the combination of optical spectroscopy with low-resolution NIR spectroscopy ($R\sim300$ and 350 in H- and K-bands, respectively) of 16 $z\sim0.2$ PSB galaxies, Zibetti et al. (2012) disfavor the TP-AGB heavy model by SSP spectral fitting. Their work shows a lack of IR excess compared to the expectations from Maraston (2005). The optical and NIR spectra are obtained from two different sources, and Zibetti et al. (2012) carried out flux calibration between the optical spectra and NIR spectra to demonstrate there was an overall NIR continuum mismatch with TP-AGB heavy models, which was their strongest argument against the importance of TP-AGB stars. Additionally, their stacked spectra do not show any evidence for the expected carbon features for TP-AGB stars at 1.41 and 1.77 μm. This seems largely consistent with our findings where we find the majority of galaxies at $z\sim0.2$ (Figure 10) are best fit by light models with some fit by mild models. This is likely due to an underlying older stellar population that is diluting spectral features from a ∼1 Gyr old stellar population where TP-AGB stars dominate. A closer look at our stacked spectra in Figure 14 reveals some evidence for a weak carbon feature at 1.1 μm, a spectral region not covered by Zibetti et al. (2012), in the spectrum best fit by TP-AGB light models, which substantiates our claim. Nevertheless, there are differences in how our sample was selected with respect to Zibetti et al. (2012) where Zibetti et al. (2012) rely on spectroscopic equivalent width (EW) criteria to carry out the selection whereas we use a color–color selection.

Another low redshift study (Riffel et al. 2015) that targets nearby spiral galaxies with AGN signatures reveals strong evidence for TP-AGB stellar features through moderate spectral resolution ($R\sim1200$) NIR spectroscopy, even though these systems were not preselected for stellar ages where TP-AGB stars are prevalent but for high S/N spectra. While these galaxies are still undergoing star formation and are presumably younger, the study detected the following TP-AGB sensitive features: TiO (0.843 and 0.886 μm), VO (1.048 μm), CN (1.1 and 1.4 μm), H_2O (1.4 and 1.9 μm) and CO (1.6 and 2.3 μm). By fitting a combination of individual stellar spectra to the galaxy spectrum, they conclude that the above features are produced by evolved stars, namely the early-AGB (E-AGB) and/or TP-AGB stars. Their work is broadly consistent with our findings where we also see a strong blended CN/TiO/ZrO feature at 0.93 μm and CN band at 1.1 μm. However, their features are likely not as strong as observed in our work due to the composite stellar populations and ongoing star formation in their sample.

More recently, Baldwin et al. (2018) observed 12 early-type galaxies at very low redshift with a broad range of ages (1–15 Gyr) and obtained moderate resolution NIR spectroscopy. They observed a lack of age variation in molecular absorption features, which seemed to indicate that either TP-AGB stars play an undersized role in galaxies or are not present at all. However, this sample consists of older passive galaxies that are not chosen to span the narrow age range where TP-AGB stars are expected to be dominant. Furthermore, they are impacted by composite stellar populations. Nevertheless, they were able to show that, for one specific galaxy in their sample with strong Balmer features, they were able to fit a Maraston & Strömbäck (2011) model, which includes TP-AGB stars, which can simultaneously fit both the strong Balmer features from archival SDSS spectra and the IR spectrum with a complex SFH.

Given that we are able to make use of both photometry and low-resolution spectroscopy for a large sample, our work has clearly demonstrated that TP-AGB stars are prevalent in PSB galaxies. The spectral stack of galaxies classified by the type of best fit model, depicted in Figure 14, clearly shows the diminishing strength of TP-AGB tracer molecular features as one moves from TP-AGB heavy to light models. This is strong evidence for the existence of these stars and the demonstration of the power of space-based low spectral resolution slitless NIR grism spectroscopy for the study of evolved stars. The overall optical/NIR continuum shape, as well as the ability to resolve molecular bands with low-resolution NIR spectroscopy, is sufficient to measure the importance of these stars. This can be an effective way to use this technique for large samples. Nevertheless, our method does have shortcomings as we are unable to fully quantify the impact of metallicity and the C/M TP-AGB ratio on the stellar spectra that we fit as we are not able to directly measure carbon and oxygen-sensitive features. Higher resolution NIR spectroscopy is required to better constrain these dependencies.

6. Summary

Our work aims to quantify the impact of TP-AGB stars by fitting the SEDs of a sample of galaxies in the redshift range $z = 0.2$–0.7. We have constructed a consistent sample of PSB galaxies through a color selection from the 3D-HST survey that contains 177 PSB galaxies. Through fitting both the ground- and space-based photometry and NIR HST grism spectra available from the 3D-HST survey with SSPs consisting of different treatments of TP-AGB stars, we have aimed to constrain the importance of the TP-AGB stars and quantify their impact on galaxy stellar mass estimates. Our conclusions are as follows:

(i) We find that ∼70% of our sample can be best fit by either TP-AGB heavy or TP-AGB mild models, which both contain significant luminosity contributions from TP-AGB stars. The remainder of the galaxies is best fit by TP-AGB light Bruzual & Charlot (2003) models.

(ii) The addition of low-resolution NIR grism spectra yields a significant improvement of model uncertainties at the spectral resolving power of HST NIR grism spectroscopy, compared to using photometry alone.

(iii) We detect molecular features associated with TP-AGB stars in the NIR grism spectra. Stacked spectra of galaxies classified either as TP-AGB heavy or mild show strong TiO/CN/ZrO blended (0.93 μm) and CN (1.1 μm) features associated with these stars.

(iv) We observe tentative evidence for an increasing fraction of galaxies best fit by TP-AGB models at higher redshifts. This is likely due to the increasing level of composite stellar populations at lower redshifts that dilute the TP-AGB contribution.

(v) We estimate that the *K*-band stellar mass estimate of PSBs can be overestimated by 0.13–0.23 dex if the contribution of TP-AGB stars to the galaxy SED is not accounted for.

The work demonstrates the power of NIR slitless grism spectroscopy in the study of evolved stars through integrated light measurements of stellar populations. Now with James Webb Space Telescope (JWST), we will be able to conduct similar studies with its slitless grism spectroscopy functionality to extend to larger samples over a broader wavelength range as well as to higher redshift.

Acknowledgments

We thank the anonymous referee for the insightful suggestions, which greatly improved the manuscript. Siqi Liu appreciates sincerely Suresh Sivanandam and Allison Man for providing ideas, insightful guidance, and suggestions. Siqi Liu thanks Ivelina Momcheva, Ros Skelton, and Gabriel Brammer for their kind help in dealing with 3D-HST spectra and photometric information, Howard Yee, Kartheik Iyer and Qing Liu for useful discussions, and also Wen-Yuan Cui, Xiao-Yan Chen for useful discussions on spectra analysis. This work is based on observation taken by the 3D-HST Treasury Program (GO 12177 and 12328) with NASA/ESA HST, which is operated by the Association of Universities for Research in Astronomy Inc., under NASA contract NAS5-26555. This work is supported by the National Natural Science Foundation of China (NSFC, Grant No. U1931209) and the National Key R&D Program of China (No. 2019YFA0405502).

ORCID iDs

Siqi Liu https://orcidorg/0000-0002-5345-4175
A-Li Luo https://orcidorg/0000-0001-7865-2648

References

Alatalo, K., Bitsakis, T., Lanz, L., et al. 2017, ApJ, 843, 9
Almaini, O., Foucaud, S., Lane, K., et al. 2007, in ASP Conf. Ser. 379, Cosmic Frontiers, ed. N. Metcalfe & T. Shanks (San Francisco, CA: ASP), 163

Baldwin, C., McDermid, R. M., Kuntschner, H., Maraston, C., & Conroy, C. 2018, MNRAS, 473, 4698
Bielby, R., Hudelot, P., McCracken, H., et al. 2012, A&A, 545, A23
Brammer, G. B., van Dokkum, P. G., & Coppi, P. 2008, ApJ, 686, 1503
Brammer, G. B., van Dokkum, P. G., Franx, M., et al. 2012, ApJS, 200, 13
Bruzual, G., & Charlot, S. 2003, MNRAS, 344, 1000
Calzetti, D. 2001, PASP, 113, 1449
Calzetti, D., Armus, L., Bohlin, R. C., et al. 2000, ApJ, 533, 682
Capozzi, D., Maraston, C., Daddi, E., et al. 2016, MNARS, 456, 790
Chabrier, G. 2003, PASP, 115, 763
Dahmer-Hahn, L. G., Riffel, R., Rodríguez-Ardila, A., et al. 2018, MNRAS, 476, 4459
Dalcanton, J. J., Williams, B. F., Lang, D., et al. 2012, ApJS, 200, 18
Dalcanton, J. J., Williams, B. F., Seth, A. C., et al. 2009, ApJS, 183, 67
Dressel, L. 2012, Wide Field Camera 3 Instrument Handbook for Cycle 21 v.5.0
Frogel, J. A., Mould, J., & Blanco, V. 1990, ApJ, 352, 96
Hinshaw, G., Larson, D., Komatsu, E., et al. 2013, ApJS, 208, 19
Iyer, K., & Gawiser, E. 2017, ApJ, 838, 127
Jin, S.-W., Gu, Q., Huang, S., Shi, Y., & Feng, L.-L. 2014, ApJ, 787, 63
Johnson, L. C., Seth, A. C., Dalcanton, J. J., et al. 2012, ApJ, 752, 95
Kajisawa, M., Ichikawa, T., Tanaka, I., et al. 2011, PASP, 63, S379
Kriek, M., Labbé, I., Conroy, C., et al. 2010, ApJL, 722, L64
Kriek, M., Van Dokkum, P. G., Labbé, I., et al. 2009, ApJ, 700, 221
Kroupa, P. 2001, MNRAS, 322, 231
Maraston, C. 2005, MNRAS, 362, 799
Maraston, C. 2012, Proc. Int. Astron. Union, 8, 272
Maraston, C., Daddi, E., Renzini, A., et al. 2006, ApJ, 652, 85
Maraston, C., & Strömbäck, G. 2011, MNRAS, 418, 2785
Marigo, P. 2015, Calibrating the role of TP-AGB stars in the cosmic matter cycle, in Why Galaxies Care About AGB Stars III: A Closer Look in Space and Time, ASP Conf., 497, 229
McCracken, H. J., Milvang-Jensen, B., Dunlop, J., et al. 2012, A&A, 544, A156
Melbourne, J., Williams, B. F., Dalcanton, J. J., et al. 2012, ApJ, 748, 47
Momcheva, I. G., Brammer, G. B., van Dokkum, P. G., et al. 2016, ApJS, 225, 27
Noël, N. E. D., Greggio, L., Renzini, A., Carollo, C. M., & Maraston, C. 2013, ApJ, 772, 58
Oke, J. B., & Gunn, J. E. 1983, ApJ, 266, 713
Retzlaff, J., Rosati, P., Dickinson, M., et al. 2010, A&A, 511, A50
Riffel, R., Mason, R. E., Martins, L. P., et al. 2015, MNRAS, 450, 3069
Schawinski, K., Urry, C. M., Simmons, B. D., et al. 2014, MNRAS, 440, 889
Schlafly, E. F., & Finkbeiner, D. P. 2011, ApJ, 737, 103
Skelton, R. E., Whitaker, K. E., Momcheva, I. G., et al. 2014, ApJS, 214, 24
Tinsley, B. M., & Gunn, J. E. 1976, ApJ, 203, 52
van Dokkum, P. G., Brammer, G., Fumagalli, M., et al. 2011, ApJL, 743, L15
Vassiliadis, E., & Wood, P. 1993, ApJ, 413, 641
Whitaker, K. E., Labbé, I., van Dokkum, P. G., et al. 2011, ApJ, 735, 86
Zibetti, S., Gallazzi, A., Charlot, S., Pierini, D., & Pasquali, A. 2012, MNRAS, 428, 1479